Quantum size effect on the optical properties of small metallic particles

Wen Chu Huang and Juh Tzeng Lue
Department of Physics, National Tsing Hua University, Hsinchu, Taiwan, Republic of China
(Received 28 January 1994; revised manuscript received 21 March 1994)

A simple quantum-sphere model for small metallic particles of arbitrary size embedded in nonabsorbing dielectric media is used to compute the real and imaginary parts of the dielectric function. The quantum confined electrons can be considered as nearly free electrons but having discrete energy levels. The dielectric function contributed from transitions between energy levels is calculated via the momentum transition matrix under the zero-temperature approximation. Consequently, we have derived the size dependence of the absorption spectra which clearly indicate the blueshift and the broadening of the spectra as the particle sizes are reduced. The theoretical simulation is in satisfactory agreement with the experimental data for particle sizes below 10 nm.

I. INTRODUCTION

The dielectric function is an important physical quantity for the study of the optical absorption spectrum of small metallic particles. Recently, much effort[1-7] has been devoted to implementing different models to solve different ranges of incident photon energies. The variational integration method as exploited in this calculation results in accurate solutions which are applicable to broad spectra.

Under the random-phase approximation, the dielectic function at low frequencies and long wavelengths is[1]

$$\lim_{\substack{\omega\to 0\\ q\to 0}} \varepsilon(q,\omega)=1+0.1061(k_F a_0)[a/a_0]^2 , \tag{1}$$

where a is the size of the particle and a_0 is the Bohr radius. However, this equation yields an infinite dielectric function as the size of the metallic particles approaches the dimensions of the bulk solid. The error mainly results from the approximation of $\omega\to 0$ and the simplified electronic transitions. Kawabata and Kubo[6] have also derived the imaginary part of the dielectric function by using the semiclassical theory of the current-current correlation function. Genzel, Martin, and Kreibig[7] obtained the dielectric function by considering the quantum degeneracy. Cocchini, Bassani, and Bourg[2] introduced a soluble tight-binding model for the simple cubic crystal to derive the dielectric function. Additionally, there are some other derivations[3-5] for the dielectric function with different approximations. But none of these calculations gives numerical results that agree with the experimental data at various sizes and frequencies.

The classical size effect presumes the correction to the dielectric function to be due to the scattering of electrons with a spherical boundary, with a reduction of the effective relaxation time by[8]

$$\tau^{-1}=\tau_b^{-1}+V_F/R , \tag{2}$$

where τ_b denotes the bulk relaxation time, V_F is the Fermi velocity, and R is the particle size. As the particle size decreases to below 10 nm, the electrons behave in a wavelike rather than a particlelike way, and the classical Drude model should be modified in some energy ranges. As the size of the metallic particles is reduced from some characteristic length to others (e.g., from the mean free path $l=V_F\tau\sim 400$ Å for silver to the de Broglie wavelength $\lambda=h/p=h/\sqrt{2mE_f}\sim 50$ Å at $E_f\sim 5.49$ eV), a microscopic size effect should appear.

In this work, the dielectric function is calculated based on quantum state transitions with wave function solved from a spherical model. The results for the blueshift and the broadening of the linewidth of the absorption spectra are comparable to the experimental data.

II. QUANTUM-SPHERE MODEL

To simplify the mathematical treatment, we propose the quantum-sphere model (QSM) for the evaluation of the dielectric function of small metallic particles. Small particles prepared by inert-gas evaporation or the chemical sol-gel process usually present a spherical shape under surface tension. The QSM infers N independent electrons confined in a sphere of radius R. We may solve the one-electron Schrödinger equation

$$H\Psi=\left[-\frac{\hbar^2}{2m}\nabla^2+V(r)\right]\Psi=E\Psi , \tag{3}$$

where $V(r)=V_0$ for $r<R$ and $V(r)=\infty$ for $r>R$. The normalized one-electron wave function is solved to be

$$\psi_{nlm}(r,\theta,\phi)=\left[\frac{2}{R}\right]^{1/2}\frac{1}{j_{l+1}(\alpha_{nl})}j_l\left[\alpha_{nl},\frac{r}{R}\right]Y_l^m(\theta,\phi)$$
$$=R_{nl}(r)Y_l^m(\theta,\phi) , \tag{4}$$

where the Y_l^m's are the spherical harmonics ($-l\le m\le l$) and j_l is the spherical Bessel function of order l with the nth root α_{nl}. The energy of the eigenstate ψ_{nlm} is

$$E_{nl}=(\alpha_{nl})^2E_0 , \tag{5}$$

where $E_0=\hbar^2/2m_e^*R^2$, m_e^* is the effective electron mass,

and the energy E_{nl} is independent of the azimuthal quantum number m.

The asymptotic approximations of the roots of the spherical Bessel functions are[3]

$$\alpha_{nl} \cong (2n+l)\frac{\pi}{2} \quad \text{for large } n \ . \tag{6}$$

The spacing of neighboring energy levels can be simplified to

$$\begin{aligned}\Delta E_l &= E_l - E_{l-1} \\ &\cong E_0[(2n+l)^2]\left[\frac{\pi}{2}\right]^2 - E_0[(2n+l-1)^2]\left[\frac{\pi}{2}\right]^2 \\ &\cong (2l+4n)E_0\left[\frac{\pi}{2}\right]^2 = \pi(E_0 E_l)^{1/2} \ .\end{aligned} \tag{7}$$

The result of a numerical estimation of E_0 is about of the order of 0.1 meV for a quantum sphere (QS) radius of $R=10$ nm, and $\Delta E_l \sim \hbar\omega$ is about 0.3 meV. As shown in Fig. 1,[9] the oscillation period of the absorption coefficient for fine aluminum particles at low temperatures is also about 0.3 meV, which clearly confirms the quantum confinement effect of the Al particles.

The dielectric function may have contributions from the terms

$$\varepsilon(\omega) = \varepsilon_\infty + \varepsilon^f + \varepsilon^i + \varepsilon^j \ , \tag{8}$$

where ε_∞ is due to positive-core-ion vibrations, ε^f is the free-carrier contribution in Drude form, ε^i is due to interband transitions, and ε^j is due to intraband transitions. For metals in the near-infrared region, the inter- and intraband transitions can be neglected, and

$$\varepsilon(\omega) \simeq \varepsilon_\infty - \frac{\omega_p^2}{\omega(\omega + i\tau^{-1})} \ . \tag{9}$$

Writing $\varepsilon(\omega)=\varepsilon_1(\omega)+i\varepsilon_2(\omega)$ and with $\omega \gg \tau^{-1}$, we obtain

$$\begin{aligned}\varepsilon_1^f(\omega) &\simeq 1 - \omega_p^2/\omega^2 \ , \\ \varepsilon_2^f(\omega) &\simeq \omega_p^2/(\omega^3\tau) \ .\end{aligned} \tag{10}$$

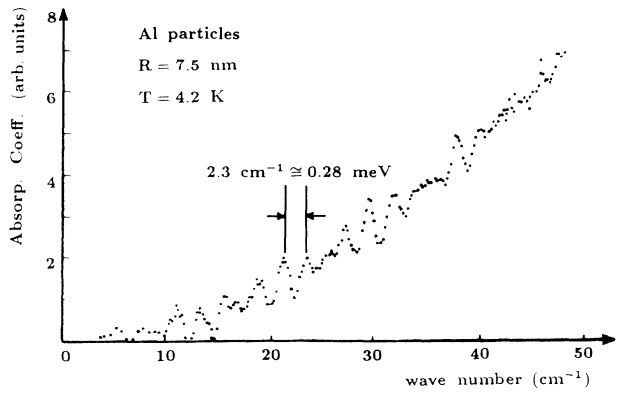

FIG. 1. Far-infrared absorption spectrum of small gas-evaporated aluminum particles with an average radius of 7.5 nm (Ref. 9).

Taking account of the classical size effect, the carrier relaxation time τ is reduced from its bulk value τ_b by the collision with the boundary. The experimental result as given in Ref. 8 indicates that the absorption coefficient is almost the same for silver at 15 and 300 K. We can take the zero-temperature approximation for the Fermi-Dirac distribution in the derivation of the dielectric function.

III. THEORY

In general, there are several methods to derive the dielectric function. Lindhard's equation is the most familiar from the point of view of many-particle physics. In quantum optics, one usually derives the electric susceptibility χ_e from the value of the matrix element of electric dipole moment μ_{mn}; then the dielectric function is equal to $1+4\pi\chi_e$. Considering the perturbation due to incident photons, the Hamiltonian is written as $(1/2m)[\mathbf{p}+(e/c)\mathbf{A}]^2+V_0$. The dielectric function evaluated in this method is[10]

$$\begin{aligned}\varepsilon^{\text{total}}(\omega,R) &= [\varepsilon_1^f(\omega)+i\varepsilon_2^f(\omega)]+[\varepsilon_1^{\text{QM}}(\omega,R)+i\varepsilon_2^{\text{QM}}(\omega,R)] \\ &= 1 - \frac{4\pi n e^2}{m\omega(\omega+i\tau^{-1})} + \frac{4\pi}{3V}\frac{1}{\hbar\omega^2}\sum_{m,n}\rho_{mn}^{(0)}|\pi_{mn}|^2\left[\frac{1}{\omega_{mn}-\omega-i\tau^{-1}}+\frac{1}{\omega_{mn}+\omega+i\tau^{-1}}\right] \ ,\end{aligned} \tag{11}$$

where V is the volume of the spherical particles, the QM represents the parts contributed from the quantum-sphere model, the indices m and n represent the filled and empty states, respectively, and $\pi_{mn}=\langle m|\hat{\pi}|n\rangle$ with $\hat{\pi}=(e/m)[\mathbf{p}+(e/c)\mathbf{A}]$; the superscript (0) denotes the zero-temperature approximation and ρ_{mm} is the Fermi-Dirac distribution for the m to n transition. The dielectric function we present here is the correction to the first order, in which the higher-order contributions of the transitions of electrons are neglected.

To simplify the calculation, we implement the bulk density of states including spin degeneracy, which is

$$D(E) = \frac{V}{2\pi^2}\left[\frac{2m_e^*}{\hbar^2}\right]^{3/2} E^{1/2} = \frac{2}{3\pi}\frac{E^{1/2}}{E_0^{3/2}} \ . \tag{12}$$

With the asymptotic approximation $\Delta E \simeq \pi(E_0 E_l)^{1/2}$, we may obtain the number of states $N(E)$ between E and $E+\Delta E$ as

$$N(E)=D(E)\Delta E \simeq 2E/3E_0 . \tag{13}$$

The real part of the dielectric function for the particles of quantum size is

$$\varepsilon_1^{\mathrm{QM}}(\omega,R)=\mathrm{Re}[\varepsilon^{\mathrm{QM}}(\omega,R)] , \tag{14}$$

where

$$\varepsilon^{\mathrm{QM}}(\omega,R)=\frac{4\pi}{3V}\frac{(4\,\mathrm{Re}E_0)^2}{(\hbar\omega)^2}\sum_{m,n}\frac{E_m E_n}{(E_m-E_n)^2}\left\{\frac{1}{[(E_n-E_m)-\hbar(\omega+i\tau^{-1})]}+\frac{1}{[(E_n-E_m)-\hbar(\omega+i\tau^{-1})]}\right\} . \tag{15}$$

In Eq. (15), we have inserted the value of the dipole matrix element

$$\pi_{mn}=\frac{e}{m}P_{mn}=\frac{4\,\mathrm{Re}E_0}{i\hbar}\frac{(E_n E_m)^{1/2}}{(E_n-E_m)} . \tag{16}$$

In evaluating this equation, we only consider the transitions near the Fermi level (i.e., $\omega_{mn}\sim 0, E_n \geq E_F \geq E_m$) and take the zero-temperature approximation of

$$\rho_{mm}^{(0)}=\begin{cases}1 & \text{if } E_m < E_F \\ 0 & \text{if } E_m > E_F .\end{cases} \tag{17}$$

For $\omega \gg \tau^{-1}$, Eq. (15) can be readily solved to yield

$$\varepsilon_1^{\mathrm{QM}}(\omega,R)\simeq\frac{4\pi}{3V}\frac{(4\,\mathrm{Re}E_0)^2}{(\hbar\omega)^2}\sum_{m,n}\frac{-2(E_n-E_m)}{(\hbar\omega)^2}\frac{E_n-E_m}{(E_n-E_m)^2}$$
$$=-\frac{32e^2E_0^2}{R(\hbar\omega)^4}\sum_{m,n}\frac{E_n E_m}{(E_n-E_m)} . \tag{18}$$

The summation in Eq. (18) can be calculated by applying the selection rule. If $E_n \geq E_F \geq E_m$, then $E_n-E_m=(2k+1)\Delta E_F$ and

$$\sum_{m,n}\frac{E_n E_m}{(E_n-E_m)}\sim E_F^2\sum_k\frac{1}{(2k+1)\Delta E_F} \quad \text{for } k=0,1,2,\ldots . \tag{19}$$

The index k includes all possible initial states, while E_m can take the values of $E_F-2k\Delta E_F$. Then

$$\varepsilon_1^{\mathrm{QM}}(\omega,R)\simeq-\frac{32e^2E_0^2}{R(\hbar\omega)^4}E_F^2 D(E_F) ,$$

where $E_0=\hbar^2/2m_e^* R^2$ and $D(E_F)=2E_F^{1/2}/(3\pi E_0^{3/2})$. Finally

$$\varepsilon_1^{\mathrm{QM}}(\omega,R)=-\frac{64}{3\pi}\frac{e^2E_F^{5/2}\hbar}{R^2(\hbar\omega)^4\sqrt{2m_e^*}} . \tag{20}$$

The same strategy can be used to solve the imaginary part of $\varepsilon^{\mathrm{QM}}$. Exploiting the identity

$$\frac{1}{x-i0+}=\mathrm{P}(1/x)+i\pi\delta(x)$$

by using the principal-value integration $\mathrm{P}(1/x)$ and the Dirac delta function $\delta(x)$, the second term in Eq. (15) vanishes owing to the presence of $\delta(x)$. Then we can replace the summation by an integral for all incident waves with $\hbar\omega \gg \Delta E \sim$ several meV. Consequently,[3]

$$\varepsilon_2^{\mathrm{QM}}(\omega,R)=\mathrm{Im}\left\{\frac{4\pi}{3V}\frac{(4\,\mathrm{Re}E_0)^2}{(\hbar\omega)^2}\int_0^{E_F}D(E)dE\int_{E_F}^{\infty}\frac{dE'}{2\Delta E'}\frac{EE'}{(E'-E)^2}\frac{1}{[E'-E-\hbar(\omega+i\tau^{-1})]}\right\}$$
$$\simeq\frac{4\pi}{3\frac{4}{3}\pi R^3}\frac{16e^2R^2}{3\pi(\hbar\omega)^4}\int_{E_F-\hbar\omega}^{E_F}E^{3/2}(E+\hbar\omega)^{1/2}dE=\frac{16}{3\pi}\frac{e^2E_F^2}{R(\hbar\omega)^3}F(\nu) , \tag{21}$$

where $\nu=E_F/\hbar\omega$ and

$$F(\nu)=\frac{1}{\nu}\int_{1-\nu}^{1}x^{3/2}(x+\nu)^{1/2}dx . \tag{22}$$

IV. NUMERICAL CALCULATIONS OF DIELECTRIC FUNCTIONS

As an example to test Eq. (20), some parameters of silver particles are given by $m_e^*=0.96m_e$, $\tau_e=3.1\times10^{-14}$ sec, and $E_F=5.49$ eV (see Fig. 2). We can demonstrate that

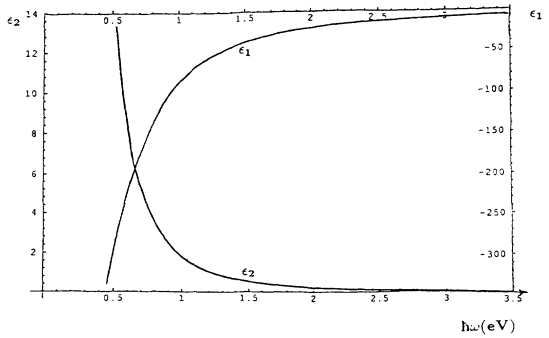

FIG. 2. Curve fitting of $\varepsilon_1(\hbar\omega)$ and $\varepsilon_2(\hbar\omega)$ with $m_e^*=0.96m_e$ and $\tau_e=3.1\times10^{-14}$ sec (Ref. 23).

$$\varepsilon_1^{\mathrm{QM}}(\omega,R)\simeq-\frac{134.8}{(R)^2(\hbar\omega)^4}\ , \tag{23}$$

where R is in units of nm and $\hbar\omega$ is in eV. Another result from Eq. (21) is

$$\varepsilon_2^{\mathrm{QM}}(\omega,R)\simeq\frac{73.68}{R(\hbar\omega)^3}\ . \tag{24}$$

For silver within the visible range of $0.5\le\hbar\omega\le3.5$ eV, $F(\nu)$ can be approximated as $(1.000-0.5034)\hbar\omega/E_F$.

The size and frequency dependence of the real and imaginary parts of ε^f, $\varepsilon^{\mathrm{QM}}$, and ε^T are shown in Figs. 3, 4, and 5, respectively. In these figures, the quantum size confinement term $\varepsilon^{\mathrm{QM}}$ approaches zero as the size $R\rightarrow\infty$. However, when the radius R is below 10 nm the values of $\varepsilon^{\mathrm{QM}}$ are comparable to those obtained from the free-electron model.

V. THEORETICAL SIMULATION OF THE ABSORPTION SPECTRA

In general, the dielectric function cannot be measured directly from experiment, while the absorption spectra can be readily measured.[11–15] For a composite system, nanocrystalline particles are embedded uniformly in a nonabsorbing matrix such as water or glass with dielectric ε_m. The absorption coefficient of the composite system can be derived from Mie's scattering as given by[16]

$$\alpha=\frac{9\varepsilon_m^{3/2}f}{c}\frac{\omega\varepsilon_2(\omega,R)}{\{[2\varepsilon_m+\varepsilon_1(\omega,R)]^2+[\varepsilon_2(\omega,R)]^2\}}\ , \tag{25}$$

where α is in units of cm^{-1} and f is the volume filling factor defined as the ratio of the volume of small particles to the total volume of particles and matrix.

In the measurement of the absorption spectra, a resonance peak occurs when

$$2\varepsilon_m+\varepsilon_1(\omega_R,R)=0\ . \tag{26}$$

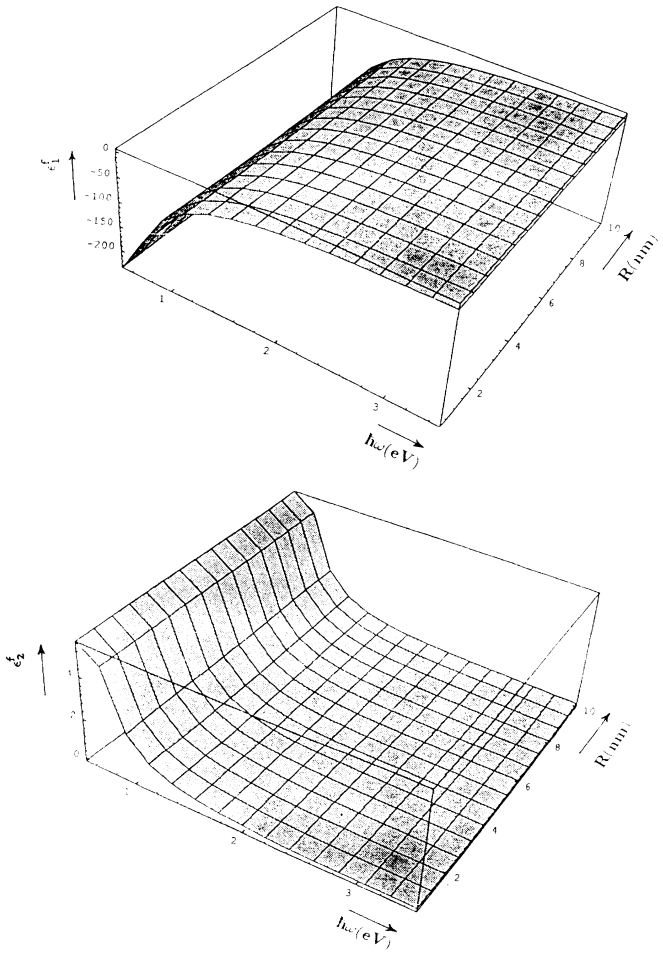

FIG. 3. $\varepsilon^f(\hbar\omega)$ is the dielectric function contributed from nearly free electrons.

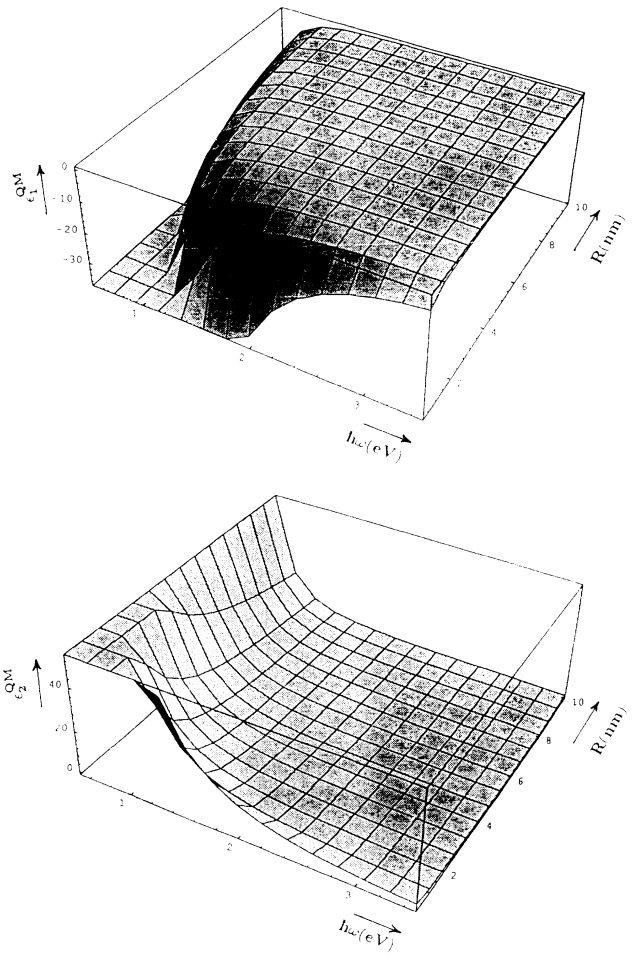

FIG. 4. $\varepsilon^{\mathrm{QM}}(\hbar\omega,R)$ is the dielectric function contributed from quantum confined electrons.

Although the absorption spectrum as derived from the Drude-like dielectric constant can satisfy the experimental data for an average diameter of about 10 nm,[17] the size dependence of the peak wavelength and half width (half width at half maximum) of the spectra cannot be predicted satisfactorily, especially when the particle size is smaller than 5 nm. Three-dimensional plots of the absorption spectra are shown in Fig. 6. As shown in Fig. 7, the peak frequency of the resonant absorption shifts to higher energy and the half width becomes larger as the particle size decreases. To find the resonance frequency for peak absorption, we may derive the frequency ω_R from the differential equation $\partial\alpha/\partial\omega|_{\omega=\omega_R}=0$. The theoretical value of ω_R for various particle sizes R obtained in this work clearly points out the trend of blueshift of the absorption spectra as shown in Fig. 8. Our derivation is based on the quantum confinement of electrons for the calculation of both ε_1 and ε_2. There are different arguments between the viewpoints of semiclassical theory[6] and quantum degeneracy.[7] The blueshift from the QSM is mainly due to the choice of an infinite barrier, by which the electron density drops suddenly from its bulk value to zero at the spherical boundary. The other argument from diffuse scattering[18,19] will predict a redshift of ω_R which can explain the experimental work of Smithard and co-workers.[14,15] But in recent years there has been some evidence[20,21] of the blueshift of ω_R. In addition to Fig. 8, we also plot Fig. 9 to compare the recent data[20] with the theory of QSM to delineate the blueshift. The deviation of the experimental values from the curve is due to the broad size distribution and the deformation of the particle shape from the ideal sphere as discussed in Ref. 20. The aspect ratio of small particles can also affect the shift of ω_R.[22] In applying the QSM to the prediction of the spectra of other metals, such as sodium, aluminum, and gold, a correct consideration of the Fermi energy as given in Eqs. (20) and (21) and the bulk contributions in Eq. (11) is required. For the absorption of near-ultraviolet light, fewer experimental results other than those of silver are available.

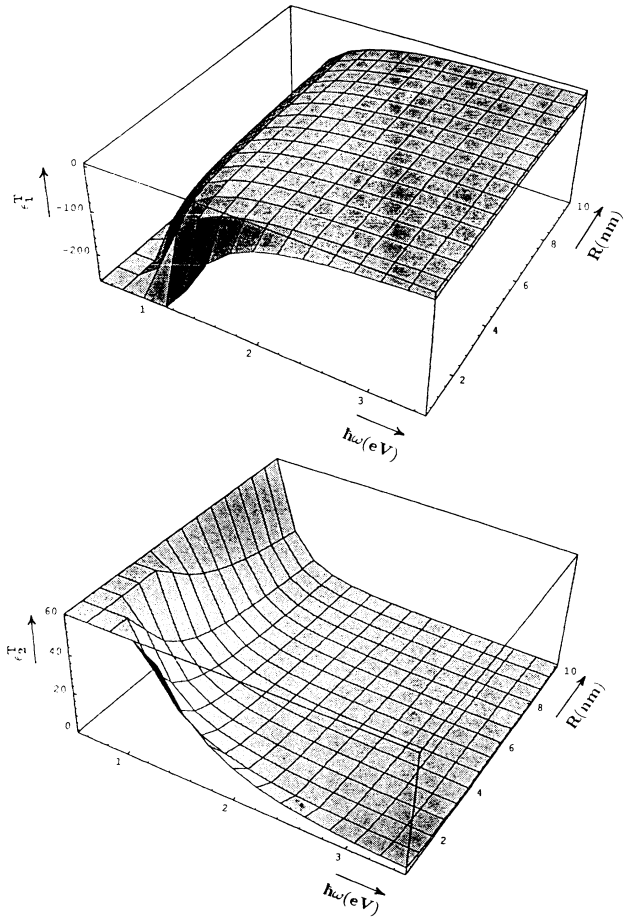

FIG. 5. $\varepsilon^T(\hbar\omega,R)=\varepsilon^f(\hbar\omega)+\varepsilon^{QM}(\hbar\omega,R)$ is the total dielectric function.

The broadening of the half width of the absorption spectrum can be derived by exploiting the Taylor expansion of α,

$$\alpha=\frac{18\pi\varepsilon_m^{3/2}f}{\lambda}\frac{\varepsilon_2(\lambda,R)}{\{[2\varepsilon_m+\varepsilon_1(\lambda,R)]^2+[\varepsilon_2(\lambda,R)]^2\}} . \tag{27}$$

The expansion near the resonance peak λ_R gives

$$2\varepsilon_m+\varepsilon_1(\lambda,R)=[2\varepsilon_m+\varepsilon_1(\lambda_R,R)]+\frac{\partial\varepsilon_1(\lambda,R)}{\partial\lambda}\bigg|_{\lambda=\lambda_R}(\lambda-\lambda_R)+\text{higher-order terms} ,$$

and the absorption coefficient α becomes

$$\alpha=\frac{18\pi\varepsilon_m^{3/2}f}{\lambda_R}\frac{\varepsilon_2(\lambda_R,R)}{\{\beta^2(\lambda-\lambda_R)^2+[\varepsilon_2(\lambda_R,R)]^2\}} , \tag{28}$$

where $\beta=\partial\varepsilon_1/\partial\lambda|_{\lambda=\lambda_R}$. From the above equation, we can obtain the half width at half maximum of the absorption spectrum as

$$\Delta\lambda_{1/2}=|\lambda_R-\lambda_{1/2}|=\varepsilon_2(\lambda_R,R)/|\beta| . \tag{29}$$

Exploiting the parameters $\lambda_p=135.1$ nm, $\lambda_0=1240$ nm, and $\lambda_R=405$ nm for silver, we can calculate

$$\beta=\frac{\partial\varepsilon_1(\lambda,R)}{\partial\lambda}\bigg|_{\lambda=\lambda_R}=\frac{\partial\varepsilon_1^f(\lambda,R)}{\partial\lambda}\bigg|_{\lambda=\lambda_R}+\frac{\partial\varepsilon_1^{QM}(\lambda,R)}{\partial\lambda}\bigg|_{\lambda=\lambda_R}\simeq-44.35-15.16/R^2 . \tag{30}$$

Consequently,

$$\Delta\lambda_{1/2}^{-1}=|\beta|/\varepsilon_2^T(\lambda_R)=\frac{44.35+15.16/R^2}{0.0623+1.847/R} , \tag{31}$$

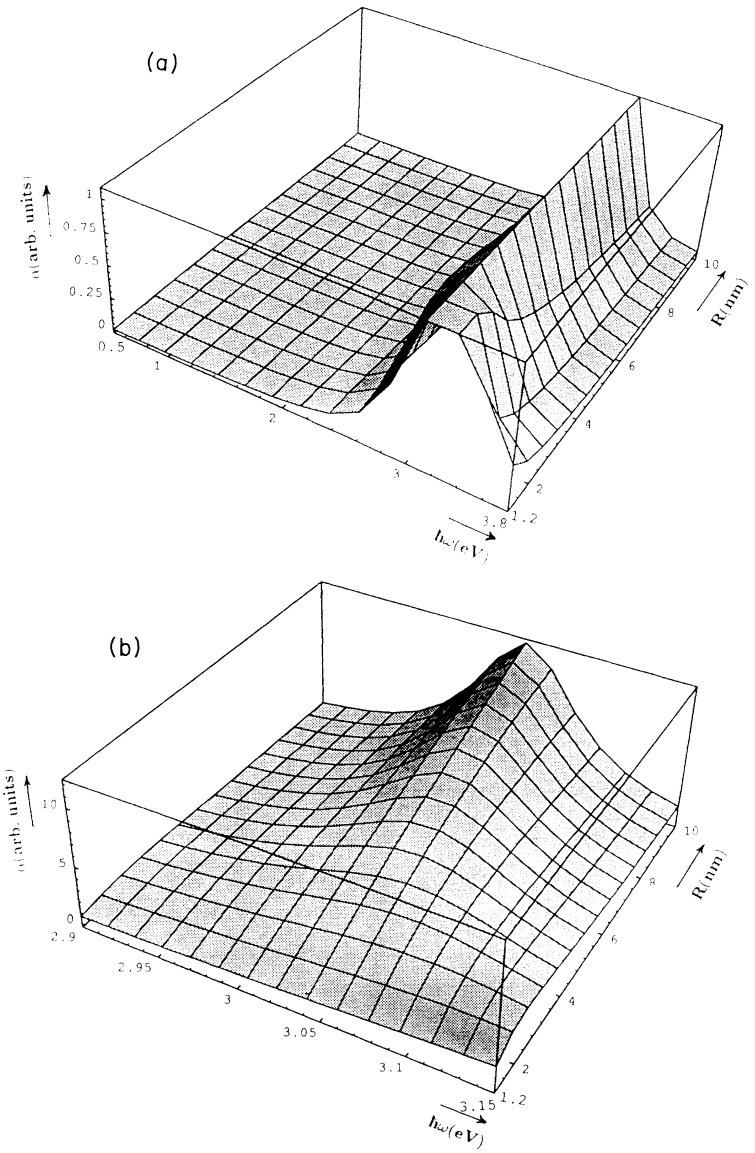

FIG. 6. (a) Three-dimensional plot of the absorption coefficient $\alpha(\hbar\omega,R)$ for $0.5\leq\hbar\omega\leq3.15$ eV and $1.2\leq R\leq10$ nm. (b) Expanded three-dimensional plot of the absorption coefficient $\alpha(\hbar\omega,R)$ for $2.9\leq\hbar\omega\leq3.15$ eV and $1.2\leq R\leq10$ nm.

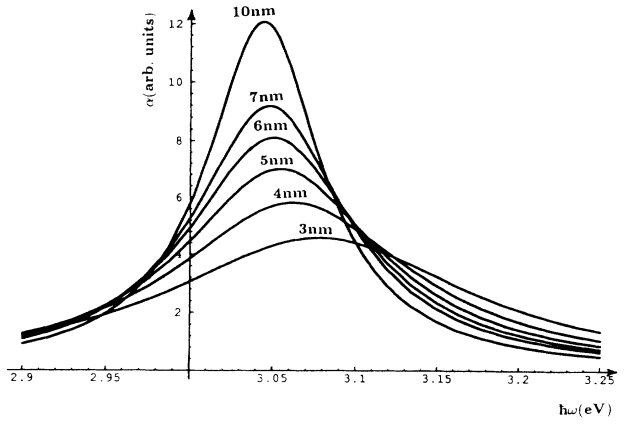

FIG. 7. Absorption spectra with different particle sizes.

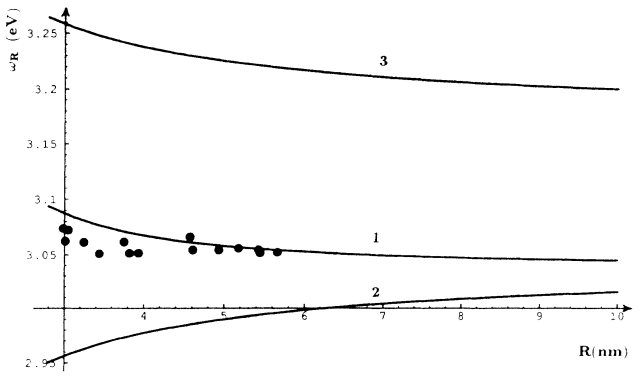

FIG. 8. Resonant absorption frequency from different calculations. Curve 1, theoretical simulation from the QSM. Curve 2, theoretical simulation from the classical size effect (Ref. 7). Curve 3, theoretical simulation from Lushnikov and Simonov (Ref. 24) by using a Thomas-Fermi screening length of 0.12 nm (Ref. 7). Points, experimental data from Genzel, Martin, and Kreibig (Ref. 7) using fine silver particles in glass.

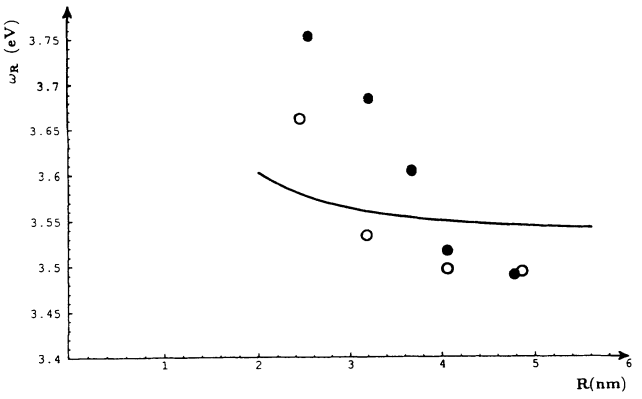

FIG. 9. Comparison of the prediction from the QSM assuming an effective $\varepsilon_m = 2.87$ (solid line) with the experimental data of Ref. 20 (circles).

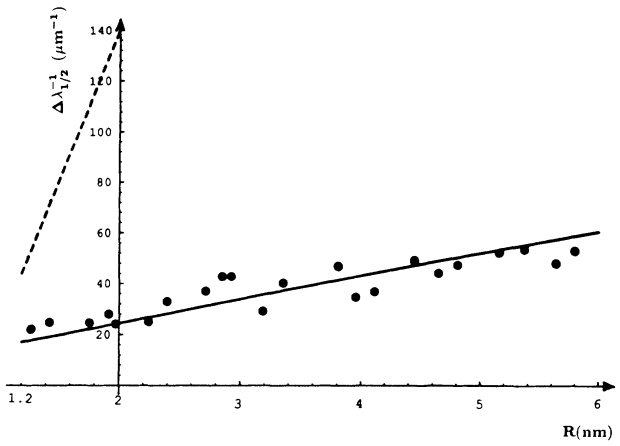

FIG. 10. Half width at half maximum of absorption spectrum. Solid curve, theoretical simulation from the QSM. Dashed curve, theoretical simulation from Kawabata and Kubo by using the semiclassical theory of the current-current correlation function (Refs. 6 and 8). Points, experimental data from Doremus (Ref. 11) and Kreibig (Ref. 12) using fine silver particles in glass.

where $\Delta\lambda_{1/2}^{-1}$ is in μm^{-1} and R is in nm. The theoretical result is indicated by the solid curve shown in Fig. 10, in which the points are the experimental data from Doremus[11] and Kreibig[12] and the dashed curve is the simulation from Kawabata and Kubo[6] using the semiclassical theory of the current-current correlation function. This quantum-sphere model yields better agreement with the experimental data than the other work.

VI. CONCLUSION

So far a serious discrepancy exists among various theories of the absorption spectra of small metallic particles. The classical size effect can explain the broadening of the half width of the spectrum, but its result is contrary to the blueshift of the resonance peak. The size dependence of $\varepsilon_1(\omega, L_{\text{eff}})$ calculated by Genzel, Martin, and Kreibig[7] can yield the approximate value of the shift of ω_R, but cannot explain the broadening of the half width of the spectrum.

In this work, we have shown that the quantum-sphere model can elucidate fully the form of $\varepsilon_1(\omega, R)$ and $\varepsilon_2(\omega, R)$ from the interband transitions of electrons. The calculated blueshift of the resonance peak and the broadening of the half width of the absorption spectrum as the size of metallic particles embedded in glass becomes smaller are satisfactorily coincident with the experimental data.[7,11–13]

ACKNOWLEDGMENTS

This work was supported by the National Science Council of the Republic of China under Contract No. NSC 83-0208-M-005-064.

[1]D. M. Wood and N. W. Ashcroft, Phys. Rev. B **25**, 6255 (1982).
[2]F. Cocchini, F. Bassani, and M. Bourg, Surf. Sci. **156**, 851 (1985).
[3]F. Hache, D. Richard, and C. Flytzanis, J. Opt. Soc. Am. B **3**, 1647 (1986).
[4]P. de Andres, R. Monreal, and F. Flores, Phys. Rev. B **32**, 7878 (1985).
[5]V. V. Truong, P. Courteau, and J. Singh, J. Appl. Phys. **62**, 4863 (1987).
[6]A. Kawabata and R. Kubo, J. Phys. Soc. Jpn. **21**, 1765 (1966).
[7]L. Genzel, T. P. Martin, and U. Kreibig, Z. Phys. B **21**, 339 (1975).
[8]W. P. Halperin, Rev. Mod. Phys. **58**, 533 (1986).
[9]D. B. Tanner, A. J. Sievers, and R. A. Buhrman, Phys. Rev. B **11**, 1330 (1975).
[10]P. N. Butcher and T. P. MacLean, Proc. Phys. Soc. London **81**, 219 (1963).
[11]R. H. Doremus, J. Chem. Phys. **40**, 2389 (1964); **42**, 414 (1965).
[12]U. Kreibig, J. Phys. F **4**, 999 (1974).
[13]H. Abe, W. Schulze, and B. Tesche, Chem. Phys. **47**, 95 (1980).
[14]M. A. Smithard, Solid State Commun. **13**, 153 (1973).
[15]J. D. Ganiere, R. Rechsteuner, and M. A. Smithard, Solid State Commun. **16**, 113 (1975).
[16]G. Mie, Ann. Phys. (Paris) **25**, 377 (1908).
[17]J. A. A. J. Perenboom, P. Wyder, and F. Meier, Phys. Rep. **78**, 173 (1981).
[18]P. Ascarelli and M. Cini, Solid State Commun. **18**, 385 (1976).
[19]P. Apell and A. Liunbert, Solid State Commun. **44**, 1367 (1982).
[20]Y. Borensztein, P. De Andres, R. Monreal, T. Lopez-Rios, and F. Flores, Phys. Rev. B **33**, 2828 (1986).
[21]M. Fujii, T. Nagareda, S. Hayashi, and K. Yamamota, Phys. Rev. B **44**, 6243 (1991).
[22]T. P. Seward, J. Non-Cryst. Solids **40**, 499 (1980).
[23]P. B. Johnson and R. W. Christy, Phys. Rev. B **6**, 4370 (1972).
[24]A. A. Lushnikov and A. J. Simonov, Z. Phys. **270**, 17 (1974).

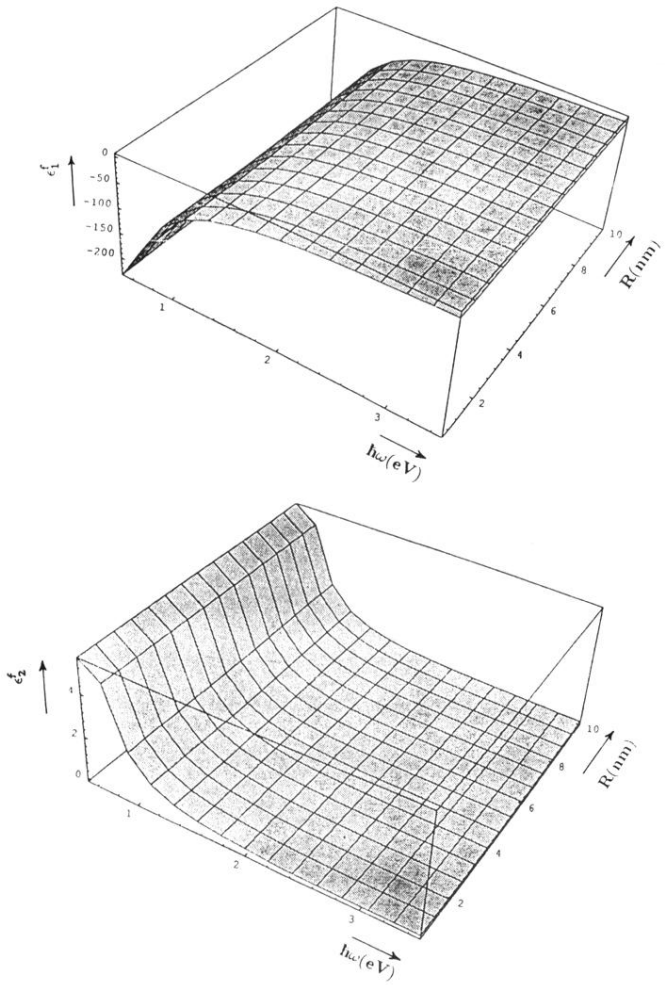

FIG. 3. $\varepsilon^f(\hbar\omega)$ is the dielectric function contributed from nearly free electrons.

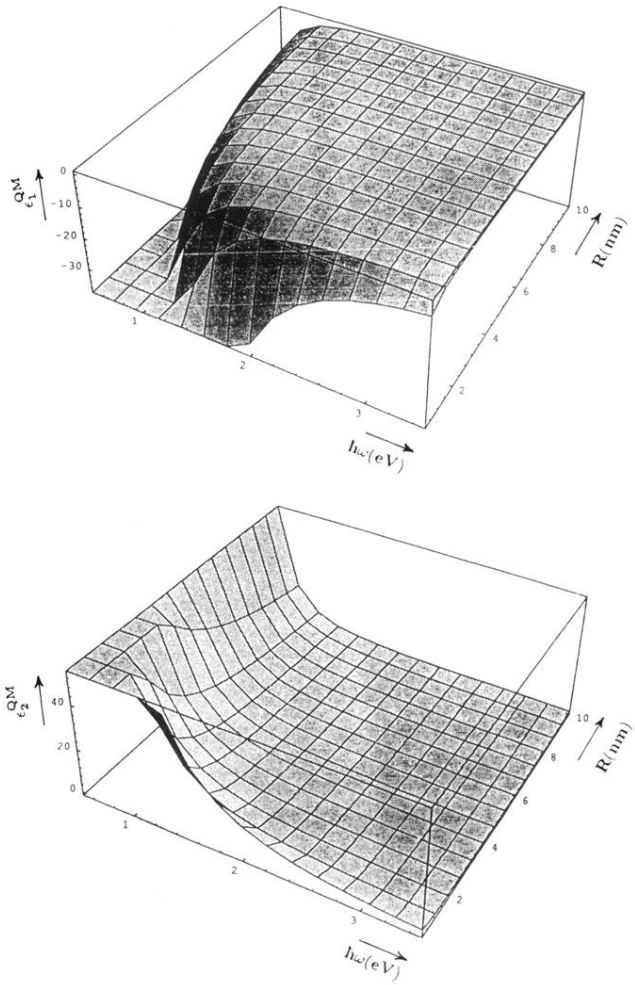

FIG. 4. $\varepsilon^{QM}(\hbar\omega, R)$ is the dielectric function contributed from quantum confined electrons.

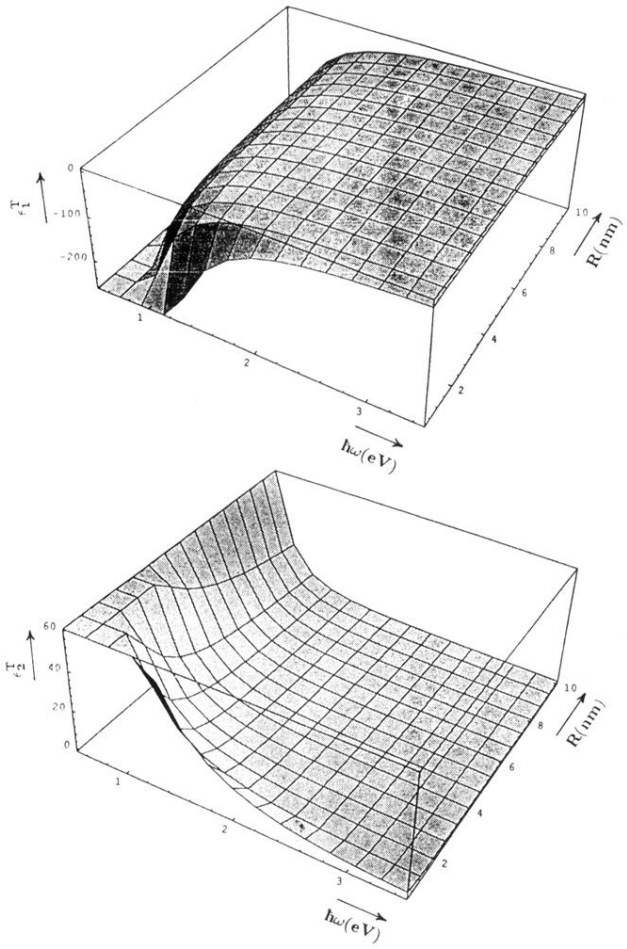

FIG. 5. $\varepsilon^T(\hbar\omega, R) = \varepsilon^f(\hbar\omega) + \varepsilon^{QM}(\hbar\omega, R)$ is the total dielectric function.

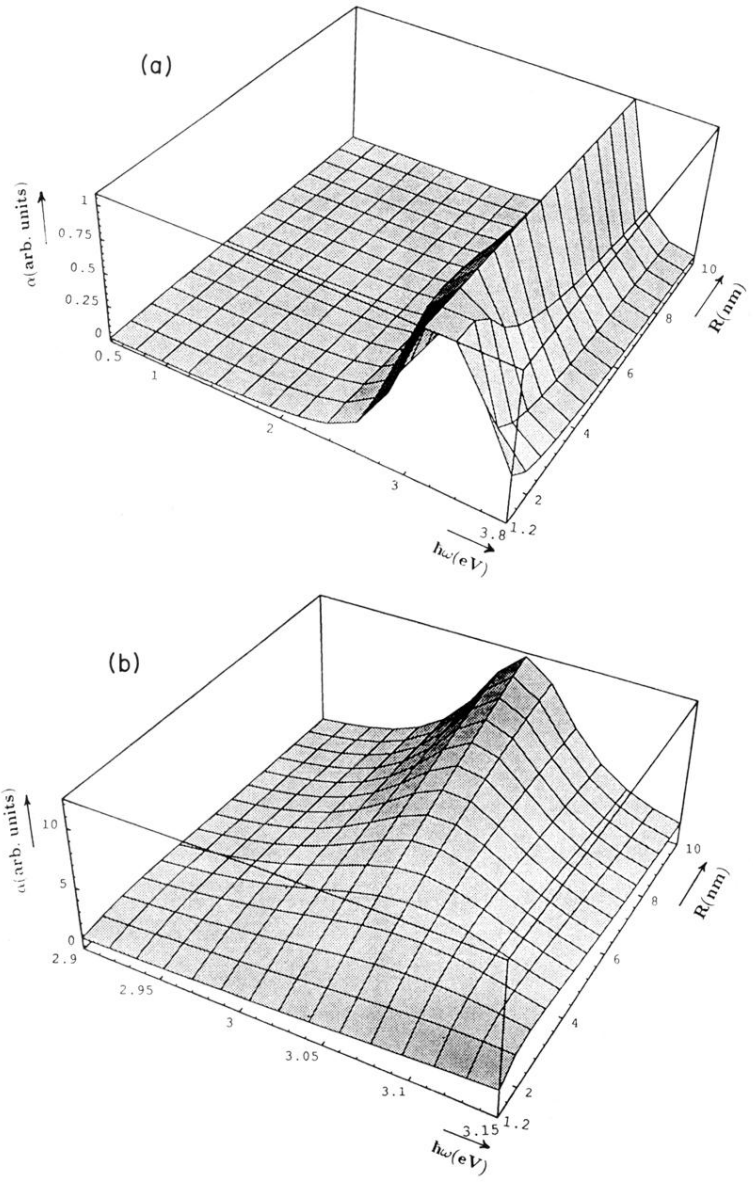

FIG. 6. (a) Three-dimensional plot of the absorption coefficient $\alpha(\hbar\omega, R)$ for $0.5 \leq \hbar\omega \leq 3.15$ eV and $1.2 \leq R \leq 10$ nm. (b) Expanded three-dimensional plot of the absorption coefficient $\alpha(\hbar\omega, R)$ for $2.9 \leq \hbar\omega \leq 3.15$ eV and $1.2 \leq R \leq 10$ nm.